A VIRTUAL RECEIVER CONCEPT FOR CONTINUOUS GNSS BASED NAVIGATION OF INLAND VESSELS

NAVITEC 2018

5-7 December 2018
ESA/ESTEC, Noordwijk, The Netherlands

Tobias Kersten, Le Ren and Steffen Schön

Leibniz University Hannover
Institut für Erdmessung (IfE)
Schneiderberg 50, D-30167 Hannover, Germany
Email: {kersten | ren | schoen}@ife.uni-hannover.de

Abstract

Efficient and economic guidance of inland vessels relies on a continuous, available, reliable and precise GNSS navigation solution. Hence, below other side effects, this is especially critical when passing beneath bridges or similar infrastructures that cross waterways. They have two effects: distortion (reflection, diffraction and interruption) of the incoming GNSS signal by the individual bridge structure on the one hand and along with that, the affected ambiguity resolution for carrier phase observation on the other hand. Thus, disturbances, discontinuities and jumps in the position estimates are present - an extreme critical situation especially for safety-relevant applications.

A multi-antenna system for marine applications combined with the concept of a virtual receiver will be presented. This approach strengthen the overall geometry of visible GNSS satellites immediately, and provides continuous position estimates even for challenging passages. Furthermore, a bridging of observations between two or more antennas on a known rigid platform reduces signal interruptions and provides continuous navigation solution under challenging or even critical environmental conditions. Laboratory experiments, driven on a 2,5 hour turn from Hannover on the Mittelland Canal on the inland vessel *MS Jenny (MS Science)* prove, that various DOP values as well as noise of the position solution are reduced significantly. The observation noise is reduced by up to 0.3–0.4 m whereby the position solution for a code based navigation reaches up to 94.5% w.r.t. classical single point positioning. The overall positioning performance is improved by up to 80%.

I. Introduction

Inland waterway transport (IWT) is an extremely reliable, almost safe and convenient option to transport freights of different kind. Hence, the versatile loading of diverse cargo reduces traffic stress on roads and motorways [1]. Motor freight ships are effective as a single vessel with dimensions of 110 m length and 10 m width provides capacity of nearly one hundred trucks or dozens of rail freight cars. Some waterways allow push tugs of up to 270 m length. However, in Europe around 6.2% [2] of total tonne-kilometres are transported on waterways. Today, infrastructure and the overall fleet condition are potential bottlenecks in IWT. Robust and reliable navigation for IWT is required to ensure safety, usability on waterways and to enable sustainable freight transport. Efficient navigation and driver assistant concepts by means of GNSS in real time kinematic mode (RTK) is a current research topic of several groups [3], [4]. The approach relies on a RTK infrastructure, which is in several cases both, even today: challenging and future-oriented, [5], [6], [7].

Passages beneath bridges or similar infrastructure crossing the waterway have two side effects that impair the code and carrier phase observations and reduce proper navigation solutions. On the one hand, signal distortions, like e.g., reflections, diffractions, which depend on the individual bridge structure, have to be considered. On the other hand, abrupt signal interruptions and complete loss-of-lock (LOL) subsequently lead to cycle slips and impair the ambiguity resolution process significantly. In general, a complete LOL could be bridged by coupling GNSS with other units such as inertial navigation systems (INS). Notwithstanding, our concept aims to be cost effective as standard infrastructure on today's vessels do not imply an INS of good quality. However, adding more than one GNSS receiver/antenna unit and selecting an optimal installation on the vessel as a rigid mobile platform is highly effective. Finally, this infrastructure is required in addition for other applications, like, e.g. the guidance in entry locks or for the assistance to find the correct docking position in harbours.

This paper presents an alternate approach, basically investigated and implemented for curved landing approaches [8], [9], [10] and satellite formation flights [11]. In this paper, we will combine a multi antenna system for marine applications [12] with the approach of a virtual receiver for an inland vessel.

II. The Virtual Receiver

Basically, the virtual receiver (VR) is a modular mathematical approach to combine code only as well as code-/carrier phase combined observations from multiple individual and optimally installed GNSS antenna/receiver combinations into a unique navigation solution. The approach can be applied to any rigid platform like e.g., satellites, air planes, vessels or ferries.

As GNSS antennas are distributed optimally on the navigation platform with known lever arm (cf. [13]), they form a kind of synthetic GNSS antenna. The field of view of such a synthetic antenna is enlarged and obstructions are reduced significantly w.r.t. a classical single antenna set-up.

Thus, dilution of precision values (DOP) and continuous navigation solution is guaranteed by this robust approach as shown for safety-relevant flight approaches [8], [9], [10]. Furthermore, this concept was extended to precise point positioning (PPP) and navigation of low earth orbiter (LEO), demonstrating that the combined carrier-/code phase solution is improved in terms of reliability, continuity and precision [11]. First marine applications are presented in [14] for the navigation of a ferry in the Galileo SEAGATE testbed in Rostock. All approaches benefit from an improved robustness and availability of observations and lead to improved navigation and position solution.

For the solution, attitude information and information about the lever arm are required. Furthermore, the correct synchronisation of each individual receiver that are connected to the distributed antennas on the platform must be considered in the modelling. Finally, the overall effect is also depending on the observation quality of the individual receiver/antenna units that are combined to a unique solution.

A. Specification for Inland Marine Application

We introduce the VR to improve the navigation solution for vessels that pass beneath bridges on a canal or river. Optimal locations for two GNSS antennas on the MS Jenny were found in the front part (FRNT) and the rear part (BACK) and are described in detail in section III-B. As conditions for signal interruptions differ between aircraft and vessel, different scenarios have to be taken into account. As the vessel moves with an approximate velocity of 10–12 km/h on the waterway, at least one GNSS antenna on the vessel provides GNSS observables to bridging the discontinuities of each individual antenna. Therefore, we combine data from the FRNT and the BACK antennas. Since the overall length of vessels is usually between 90–125 m, baseline lengths of approx. 60 m are considerable long enough to cover most cases of signal interruptions at individual antennas.

In general, as the lever arm is known with position precision, the reference of the VR can be chosen arbitrarly. In our investigation, we used the location of the FRNT antenna.

B. Mathematical Concept

The observation equation P_B^k of the BACK antenna B to a k^{th} satellite gets

$$P_B^k = \sqrt{(X^k - (x_{vr} - \Delta x))^2 + (Y^k - (y_{vr} - \Delta y))^2 + (Z^k - (z_{vr} - \Delta z))^2} + \delta t_B + \epsilon \tag{1}$$

with the Earth Centred Earth Fixed (ECEF) vector of the satellite $[X_i^k]^T = (X^k, Y^k, Z^k)$, the position of the VR $[x_{vr_i}]^T = (x_{vr}, y_{vr}, z_{vr})$ and the lever arm between both antennas on the platform $[\Delta x_i]^T = (\Delta x, \Delta y, \Delta z)$, the receiver clock estimate δt_B and ϵ the dumped remaining effects such as satellite clock estimates, ionospheric effects and others. Similarly, we found the observation equation P_F^k for the FRNT antenna F including the individual receiver clock estimates δt_F and dumped remaining effects ϵ which reads

$$P_F^k = \sqrt{(X^k - x_{vr})^2 + (Y^k - y_{vr})^2 + (Z^k - z_{vr})^2} + \delta t_F + \epsilon \tag{2}$$

which results in the design matrix A for the epoch wise least-squares adjustment (LSA),

$$A = \begin{bmatrix} -\frac{\partial P_B^1}{\partial x_{vr}} & -\frac{\partial P_B^1}{\partial y_{vr}} & -\frac{\partial P_B^1}{\partial z_{vr}} & 1 & 0 \\ \vdots & \vdots & \vdots & \vdots & \vdots \\ -\frac{\partial P_B^k}{\partial x_{vr}} & -\frac{\partial P_B^k}{\partial y_{vr}} & -\frac{\partial P_B^k}{\partial z_{vr}} & 1 & 0 \\ \cdots & \cdots & \cdots & \cdots & \cdots \\ -\frac{\partial P_F^1}{\partial x_{vr}} & -\frac{\partial P_F^1}{\partial x_{vr}} & -\frac{\partial P_F^1}{\partial x_{vr}} & 0 & 1 \\ \vdots & \vdots & \vdots & \vdots & \vdots \\ -\frac{\partial P_F^k}{\partial x_{vr}} & -\frac{\partial P_F^k}{\partial x_{vr}} & -\frac{\partial P_F^k}{\partial x_{vr}} & 0 & 1 \end{bmatrix}. \tag{3}$$

As shown by Eq. (3), the synchronisation of the two individual receiver time scales extend the design matrix and five parameters have to be estimated per epoch.

(a) Laboratory navigation platform *MS Jenny*

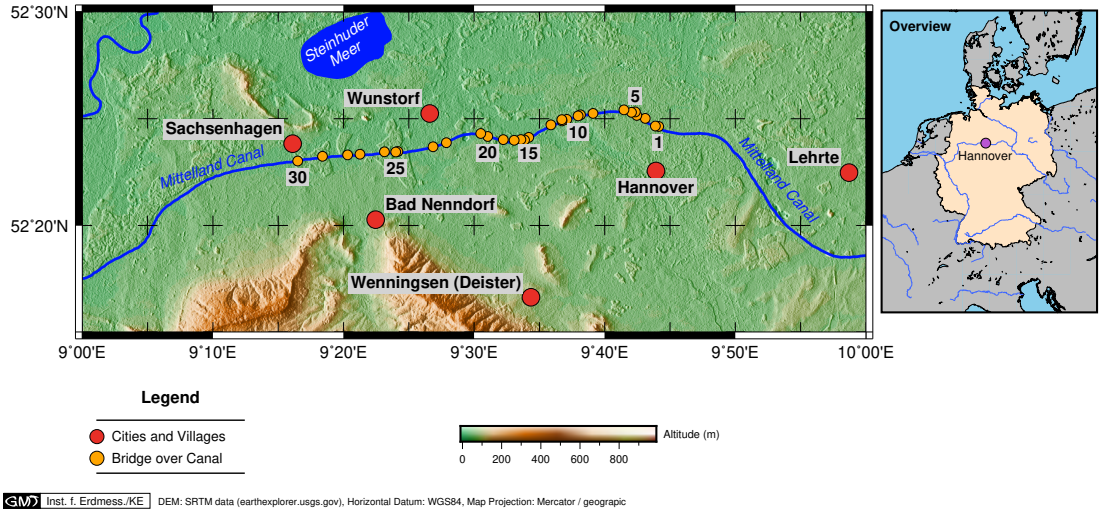

(b) Trajectory with passed bridges and infrastructures

Figure 1. Inland vessel *MS Jenny* during the kinematic session on June 27, 2016. Locations of the receiver and antennas are indicated by FRNT (front of the vessel) and BACK (back of the vessel) (a), geo-referenced trajectory of kinematic session showing passages of infrastructure that crosses the canal (b).

III. Application to Inland Vessels

A. The Inland Vessel MS Jenny

The motor freight ship MS Jenny (cf. Fig. 1(a)) is modified to an event and exhibition vessel and provides optimal conditions for GNSS laboratory applications. As also known by the name *MS Science*, this vessel annually travels on behalf of the Federal Ministry of Education and Research (Germany) with changing exhibitions through Germany and partly Austria as a *swimming science centre*. The geometric dimensions of the vessel are: 100 m length, 9.5 m width and 3.16 m depth. The overall capacity is 72 TEU with a carrying capacity of 2290 TWD by an engine power of 809 kW. The on-board satellite navigation unit is a Radarpilot 720°.

B. Hardware set-up

In June 2016 and June 2018 several datasets were captured. This paper will focus on a campaign from June 27, 2016 (DOY 179). There, two datasets have been recorded. The first dataset was captured for one hour as the vessel lays at the mooring point cf. [15] for more details. The second dataset was captured during a trip from Hannover westward on the Mittelland Canal for 2.5 hour (cf. Fig. 1(b)) and is assigned to be the *kinematic session*. The trajectory of the kinematic session provides a travelled distance of approximate 35 km. During this time, the vessel passes beneath 30 bridges and infrastructures.

Two individual GNSS receivers were mounted at pillars on-board the vessel as depicted in Fig. 1(a). The marker of the front receiver (Javad Delta TRE-G_G3T) is defined as FRNT, the back receiver (Novatel SPAN-SE) is named BACK. The data record interval is 1 Hz. The two receiver were operated with identical GNSS antennas (NOV702GGG.R2). To prove and control the precision of the lever arm, individual methods (RTK and total station) were used to compute the vector between FRNT and BACK, as $|[\Delta x_{bf_i}]^T| = 57.34\,\text{m}$ with corresponding standard deviation of $\sigma_{\Delta x} = \pm 0.02\,\text{m}$.

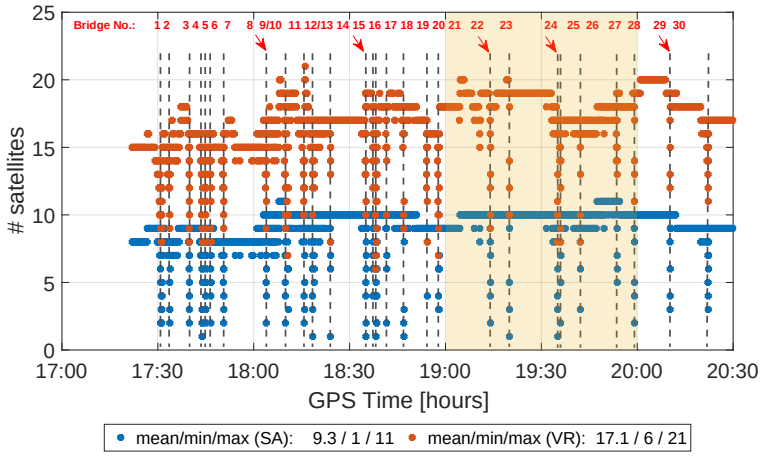

Figure 2. Number of visible satellites for VR and SA during kinematic session. Bridge passages are indicated by dashed lines and strongly reduced satellite visibility.

C. Processing strategy

A single antenna code based solution (SA) is processed with our own software for the FRNT antenna and is compared to the virtual receiver (VR) solution with focus on availability, continuity, accuracy and precision. The lever arm between BACK and FRNT antenna is defined in the vessel body frame (VBF) and transformed to the ECEF. In a first step, we use the heading that is obtained from a moving baseline solution (obtained by Novatel GrafNav, Vers. 8.50.4923). Furthermore, the transport rate is considered. We assumed the vessel as a rigid platform. However, in reality a vessel is not a rigid platform and this fact should be considered in future precise processing. Hence, a higher observation noise is expected for this investigation. Position estimates are computed for different weighting schemes and with an elevation cut-off angle of 2°.

IV. Results

A. Satellite Visibility

In Fig. 2 the overall satellite visibility over time and for all 30 bridge passings is depicted for both, the SA and the VR solution. The mean number of visible satellitesis 17.1 for the VR case and 9.3 for SA. As expected, for all 11014 epochs, the number of usable satellites for VR is at every epoch higher than for SA. Bridge passings are indicated by grey dashed lines and the corresponding bridge number. A strong reduced number of visible satellites is detectable at those positions. However, in the case of VR a minimum number of at least 6 satellites is visible and usable.

To guarantee position and fault detection (FDE) a minimum number of 6(7) satellite in the case of SA(VR) must be available. For VR this is fulfilled in 99.2% of all epochs, for SA in 97.4%. Cases, where no position solution is provided amount to 0.8% in the case of VR, whereby for SA this raises to 2.5%. In addition, a sufficient number of usable satellites is available for the VR even at difficult locations and situations, i.e. when several bridge passings are very close and short to each other.

B. Dilution of Precision (DOP)

Generally, the quality of receiver location is characterised by two major parts, the user range error (URE) and the navigation geometry. As long as errors are identically distributed over all visible satellites, the error due to geometry mapped into position

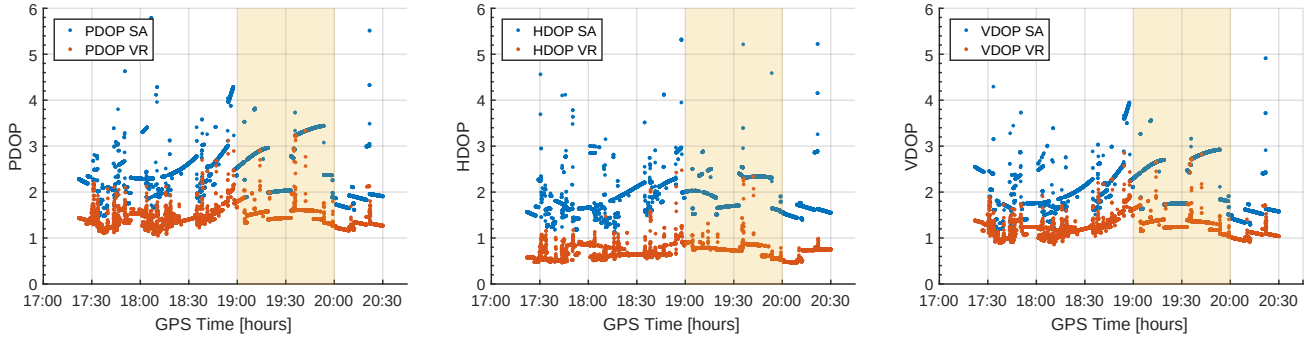

(a) (b) (c)

Figure 3. Comparison of usable GNSS satellites and geometry quality for the determination of position estimates of SA and VR approach shown by means of various DOP values. Depicted are the overall Position-DOP [*PDOP*] (a), the topocentric Horizontal DOP [*HDOP*] (b) and Vertical DOP [*VDOP*] (c).

Table I
STANDARD DEVIATION OF THE NAVIGATION SOLUTION OBTAINED BY VR AND SA APPROACH FOR KINEMATIC SESSION. RESULTS REFER TO COS2 WEIGHTING.

	Mean values [m]				**Standard Deviations [m]**			
	ΔN	ΔE	ΔU	ΔPOS	$\sigma\Delta$N	$\sigma\Delta$E	$\sigma\Delta$U	$\sigma\Delta$POS
VR	0.337	-0.605	-0.335	0.737	0.565	0.243	0.427	0.584
SA	0.867	-0.570	-0.620	1.293	0.657	0.390	0.674	0.917

is extracted by the position dilution of precision (PDOP), [16], [17]. Hence, these values are collected in Fig. 3 for both cases of SA and VR. As the PDOP refers to the quality of the estimated position unknowns, Fig. 3(a) shows, that the VR positioning outperforms the classical SA position estimation for the complete track of 2.5 hours on the Mittelland Canal.

The most significant improvement is noticeable in the HDOP (Fig. 3(b)) and further improvements are to find for the VDOP (Fig. 3(c)). Bridge passings remain difficult, as for the cases of the VR the DOP values also suddenly enlarge to higher values due to a difficult geometry. However, the effect is definitely smaller than for the cases of SA and proves, that the geometry of visible satellites is consequently improved or even strengthened. Clearly we have shown that for the VR all DOP values are significantly smaller than for the SA case, caused by the enlarged field of view of the synthetic antenna. Hence, available observations are consequently coordinated to a combined solution.

C. Accuracy

To obtain the position solution, three different observation weighting approaches were processed and compared to a reference solution: identical weighting (IDEN), elevation dependent weighting (COS2) and C/N0 based weighting (CN0), [18]. The reference solution is obtained by a carrier phase based ionosphere free (L3) double difference approach, whereby the reference station is located at our rooftop GNSS laboratory in Hannover. The reference is processed with GrafNav using precise products from the center of orbit determination (CODE) [19]. To acquire a measure for accuracy and precision, we compute for all weighting schemes the position error (PE) by

$$\Delta\hat{x} = \hat{x} - x \tag{4}$$

with x being the reference trajectory, and $\hat{x}$ the SA or VR, respectively. The estimated components and their corresponding quality parameters are collected in Tab. I. Here, it is shown, that the deviation in a local topocentric system based in the reference trajectory is significantly smaller for the VR case in nearly all coordinate components and that the noise of the position estimation is reduced in addition.

Focussing on the horizontal position error (HPE)

$$\text{HPE} = \sqrt{(\Delta\hat{x}_N^2 + \Delta\hat{x}_E^2)} \tag{5}$$

and the absolute values for the vertical error (VPE)

$$\text{VPE} = |\Delta\hat{x}_U| \tag{6}$$

which are shown both in Fig. 4 strengthen these findings accordingly. The time series of SA and VR positions are noisy as we omit any further carrier phase based code smoothing to precisely study the effect of bridge passings on the captured observables. Fig. 4 furthermore shows, that signal interruptions due to bridge passings are present and visible by peaks and sudden jumps in both solutions. The VR outperforms the SA solution with significant smaller HPE and VPE. Here, HPE-values of 0.72 m are achieved for the VR. In the case of SA they are around 0.97 m at the same time. Similar performance is detected for the VPE. For the VR case, a RMS of 0.48 m is determined and a much larger magnitude (0.71 m) for the SA case. At least, if focussing on the specific time at around 19:00 o'clock (orange bar), where a very challenging geometry is present, the VR solution has less HPE and VPE than the corresponding SA solution. Tab. II lists details for all processed weighting approaches. Although it was assumed that a C/N0 based weighting of observations would improve both, VR and SA approach as diffraction and scattering due to the vicinity of the bridges are taken into account, we obtained the optimal solution using the COS2 weighting (cf. Tab II).

D. Position Availability

In terms of availability, the VR solution improves the availability significantly. Hence, for the case of SA, no solution was possible for 2274 epochs out of 11014 which represents an availability of 80.3%, whereby in the case of VR the number of epochs with no precise position solution decreases to 635 epochs, i.e. 94.5%.

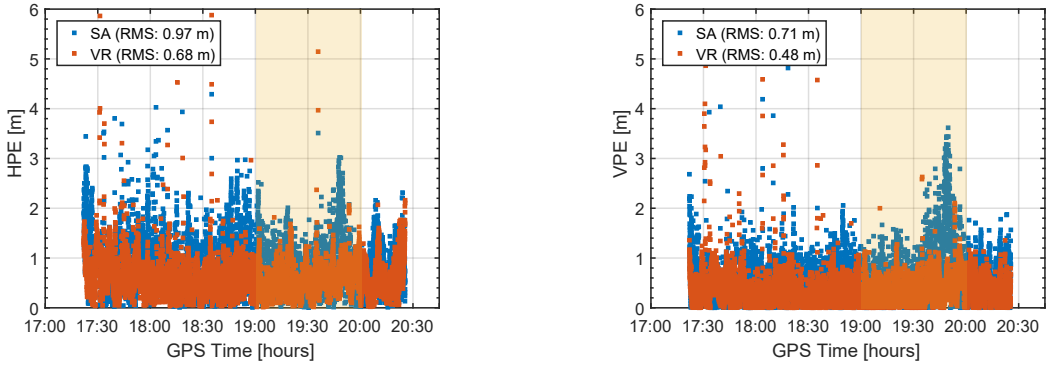

(a) (b)

Figure 4. Comparison of accuracy w.r.t. carrier phase based DD reference trajectory. Solutions are obtained for the kinematic session and with COS2 weighting for the SA and VR approach with the horizontal position error (HPE) in (a), vertical position error (VPE) in (b).

Table II
COMPARISONS OF DIFFERENT PROCESSING WEIGHTINGS ON THE OVERALL PERFORMANCE OF THE VIRTUAL RECEIVER (VR) CONCEPT.

	VR			**SA**		
	IDEN	COS2	CN0	IDEN	COS2	CN0
HPE [m]	0.76	0.68	0.77	1.03	0.97	1.09
VPE [m]	0.49	0.48	0.53	0.78	0.71	0.76
Availability [%]	93.7	94.5	94.2	80.3	76.7	75.8

To summarize these findings, a VR approach significantly improves the availability of positioning with minimal effort due to an optimal distribution of GNSS antennas on a vessel. However, there will be few and short discontinuities, too. Fig. 4 underlines the findings (cf. Sec. IV-A) as there are several VR positions provided where a SA solution was not possible.

V. DISCONTINUITIES

Discontinuities caused by bridges or similar structures above canals are complex for code and carrier phase based positioning and are studied in detail in this section. As the code observables could be repaired easily by bridging the observations in the close vicinity of the bridges passed by pivoting one antenna on the vessel and determine a VR solution, most difficulties occur for the carrier phase. A study of the carrier-to-noise (C/N0) and corresponding multipath linear combination (MP) gives the insights.

A. Carrier to Noise and Multipath Linear Combination

For a specific study, we zoom into the timespan between 19:00 and 20:00 for both, the FRNT and BACK antenna. During this time, the vessel passed beneath seven bridges of individual kind of construction, namely number 22–28. Tab. III gives an outline of the details of these bridges. The Fig. 5 summarizes the C/N0 and corresponding multipath linear combination on C/A (MP1), generated from the RINEX-3 observation specifiers GC1C and GL1C and GL2W, [20]. The consistency of the GNSS observables at the close vicinity of the appearing bridge can be evaluated along with the multipath linear combination (MP), [21], [22].

Different C/N0 characteristics of the FRNT and BACK receiver are remarkable (cf. Fig 5(a) and 5(c)) as different receiver types (cf. Sec.III-B) were used for both locations.

The corresponding MP1 confirm the individual behaviour for the receiver types. They are depicted both in Fig. 5(b) and Fig. 5(d). The BACK receiver uses enhanced carrier phase based code smoothing whereby the FRNT receiver does not. Therefore, bridge passages of very thin infrastructures are hard to detect in the C/N0 or the corresponding MP1 of the BACK antenna.

B. Bridge Passages in Detail - Discussion

Bridge passages are indicated by sudden drops of the C/N0 values. Depending on the satellite elevation, drops of up to 20 dB-Hz occur. The overall MP1 for the FRNT receiver shows systematic variations. Bridge passages lead to sudden jumps of MP1 of up to ±3–4 m (e.g. for bridges 23, 24 or 25). caused by cycle slips on one of the frequencies (whether GL1C or GL2W). These effects show up several time for both receiver (FRNT and BACK). These challenges are also occurring for

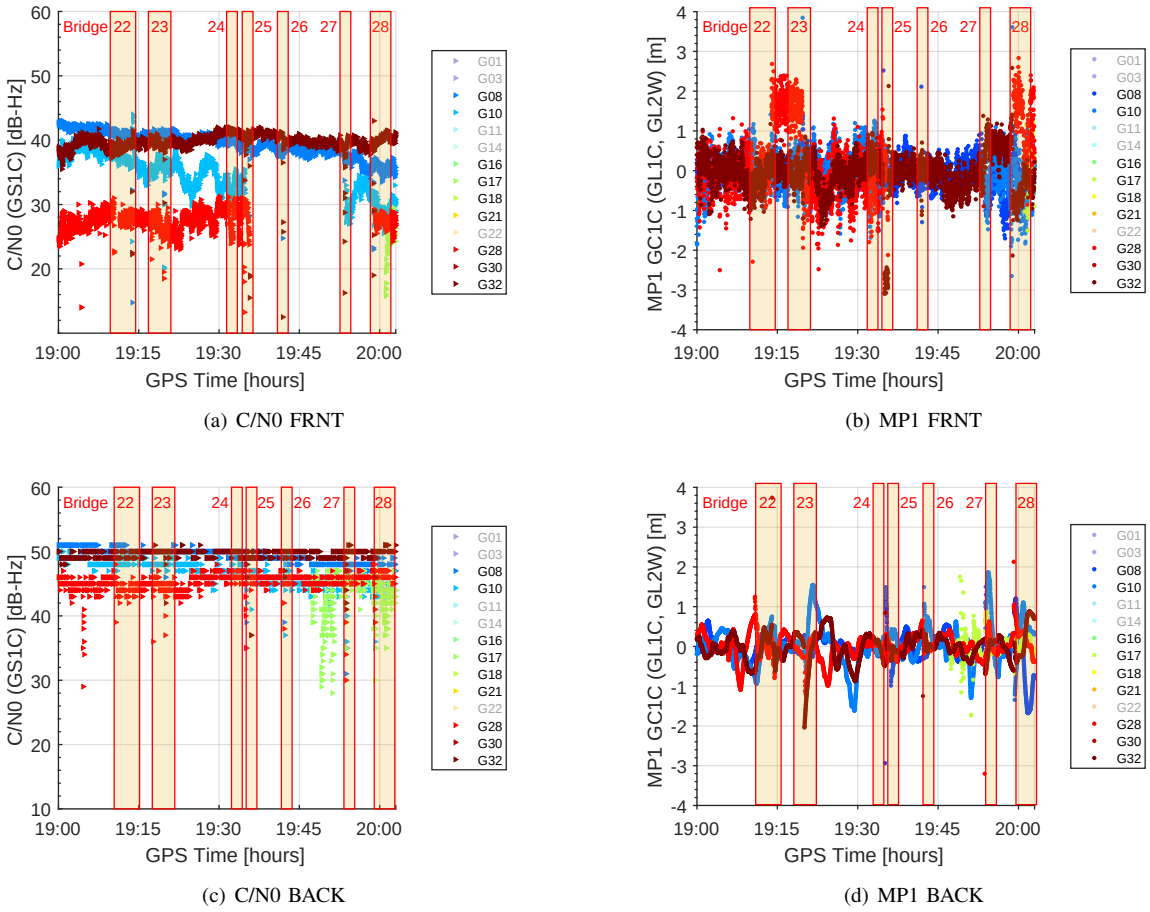

(a) C/N0 FRNT

(b) MP1 FRNT

(c) C/N0 BACK

(d) MP1 BACK

Figure 5. Discontinuities in terms of C/N0 and multipath linear combination MP1 GC1C (GL1C, GL2W) exemplary shown for selected satellites with challenging visibility for the FRNT and BACK GNSS antenna for a selected time span of the kinematic session.

Table III
BRIDGE PASSAGES FOR A ONE HOUR TIME SPAN BETWEEN 19:00 AND 20:00 O'CLOCK, KINEMATIC SESSION

Bridge No.	**Function**	**Lanes**	**Form**	**Time of Arrival (FRNT)** [hours]	**Width** [m]	**Travelled distance under bridge** [m]
22	car	2	flat	19:14	15	15
23	farm lane	1	flat	19:19	8	8
24	railway	2	metal arc	19:35	13	17
25	cars	2	flat	19:35	13	14
26	pedestrian	1	metal arc	19:42	6	6
27	car	2	metal arc	19:53	8	8
28	car	1	metal arc	19:59	5	5

RTK approaches and have to be considered as discussed in [7]. A passage of a bridge leads to a complete LOL and requires a ambiguity re-initialisation. This process needs further knowledge from outside, otherwise, the ambiguities of the carrier phase solution are scattered by each bridge passage.

At the BACK receiver, the conditions are completely different. Although, bridge passages are indicated by sudden interrupts of C/N0, the corresponding MP1 in Fig. 5(d) are very smoothed and show small magnitudes for MP1. But the smoothing leads to discontinuities, too. This is indicated e.g., at bridge 23 for the satellite G32 or even more visible at bridge 23 and between 24/25 for the G10. However, differences between FRNT and BACK receiver are detectable w.r.t. the visibility of G28. This satellite is not recorded at the FRNT receiver between bridge passage 25 and 28. At the BACK receiver this satellite could be recorded without any discontinuity, although both antennas are installed at the same high and bore side of the vessel.

VI. Conclusion

In this paper, we presented the VR as a concept. The combination of several GNSS receiver antennas, which are optimally distributed on a mobile platform, lead to a unique synthetic antenna with a significantly enhanced field of view. The paper showed, that for bridge passings of inland vessels, the interruptions of GNSS positioning are reduced dramatically with respect to a classical SA approach. The geometry of visible satellites is improved too, as an overall minimum number of six satellites is available at any time. This is proven by the significantly reduced HPE and VPE, which amount up to 0.3–0.4 m. Furthermore, the availability of GNSS positioning is improved for navigation of inland vessels that pass beneath bridges and other infrastructure above canals from 76.7% (SA case) up to 94.5% (VR case).

Acknowledgement

The investigations of this project were driven by a one-year student project seminar on the topic of Navigation and Positioning at the Leibniz University Hannover. Therefore, the authors like to thank in addition all the contributors for this valuable project, namely Lucy Icking, Sara Brakemeier, Arman Kharma, Fabian Ruwisch and Vahid Aghajani.

Furthermore, we like to acknowledge the Center of Orbit Determination in Europe for providing precise orbit and satellite products.

At least, very special and warm thanks I like to dedicate to the captain of the *MS Jenny* (*MS Wissenschaft*) Albrecht Scheubner and his wife for their grateful support and interest on this project and their familiar hosting during the GNSS campaigns.

References

[1] W. Sihn, H. Pascher, K. Ott, S. Stein, A. Schumacher, and G. Mascolo, "A Green and Economic Future of Inland Waterway Shipping," *Procedia CIRP*, vol. 29, pp. 317–322, 2015.

[2] Eurostat. (2018) Modal split of freight transport in Europe. [Online]. Available: https://ec.europa.eu/eurostat/statistics-explained/index.php/Freight_transport_statistics_-_modal_split

[3] D. Medina, A. Heßelbarth, R. Büscher, R. Ziebold, and J. García, "On the Kalman Filtering Formulation for RTK Joint Positioning and Attitude Quaternion Determination," in *IEEE/ION PLANS 2018*, 2018. [Online]. Available: https://elib.dlr.de/119912/

[4] A. Heßelbarth, R. Zeibold, M. Sandler, J. Alberding, M. Uhlemann, M. Hoppe, M. Bröschel, and L. Burmisova, "Towards a Reliable Bridge Collision Warning System for Inland Vessel Navigation Based on RTK Height Determination," in *Proceedings of the 30th International Technical Meeting of The Satellite Division of the Institute of Navigation (ION GNSS+ 2017)*, Sep. 2017, pp. 1866–1885. [Online]. Available: https://elib.dlr.de/114704/1/Abstract_ION.pdf

[5] L. Wanninger, "Virtuelle GPS-Referenzstationen für großräumige kinematische Anwendungen," *ZfV*, vol. 128, no. 3, pp. 196–202, 2003. [Online]. Available: http://geodaesie.info/zfv/heftbeitrag/1408

[6] M. Hoppe, "GNSS-Anwendungen in der Schiffahrt," in *157. DVW-Seminar*, ser. Schriftenreihe des DVW, vol. 87. Wißner-Verlag, Feb. 2017, pp. 93–105. [Online]. Available: http://geodaesie.info/sr/beitrag/gnss-anwendungen-der-schifffahrt/6363

[7] A. Heßelbarth, "GNSS in der Hydrographie," in *170. DVW-Seminar und 32. Hydrographentag*, ser. Schriftenreihe des DVW, vol. 91. Wißner-Verlag, Juni 2018, pp. 47–64. [Online]. Available: https://elib.dlr.de/120442/

[8] F. Kube, S. Schön, and T. Feuerle, "Virtual receiver to enhance GNSS-based curved landing approaches," *Proceedings of ION GNSS 2011, Portland, Oregon, USA*, pp. 536–545, 2011.

[9] F. Kube, S. Schön, and T. Feuerle, "GNSS-based curved landing approaches with a virtual receiver." IEEE, 2012, doi: 10.1109/PLANS.2012.6236880.

[10] F. Kube, S. Schon, and T. Feuerle, "Improved navigation performance for curved approaches with a virtual receiver," in *2012 6th ESA Workshop on Satellite Navigation Technologies (Navitec 2012) & European Workshop on GNSS Signals and Signal Processing*. IEEE, 2012.

[11] F. Kube, C. Bischof, P. Alpers, C. Wallat, and S. Schön, "A virtual receiver concept and its application to curved aircraft-landing procedures and advanced LEO positioning," *GPS Solutions*, vol. 22, no. 2, p. 41, Feb 2018. [Online]. Available: https://doi.org/10.1007/s10291-018-0709-y

[12] V. Böder, "Zur Hochpräzisen GPS-Positions- und Lagebestimmung unter besonderer Berücksichtigung mariner Anwendungen," phdthesis, Wissenschaftliche Arbeiten der Fachrichtung Vermessungswesen der Universität Hannover, 2002.

[13] S. Nair and C. Bartone, "Multiple antenna GPS configuration for enhanced performance," *Proceedings of ION AM, Institute of Navigation, June 7-9, Dayton, Ohio, USA*, pp. 188–199, 2004.

[14] S. Schön and P. Alpers, "A Virtual receiver for Pseudolites: Enhancing the positioning and Heading Determination of a Ferry," in *Proc ION GNSS+ Miami Florida, 24.-26.9.2018*, 2018.

[15] T. Kersten, L. Ren, and S. Schön, "Continuous Navigation of an Inland Vessel with a Synthetic GNSS Antenna," in *DGON-Symposium Positionierung und Navigation für Intelligente Verkehrssysteme*. DGON, 2018.

[16] P. Massat and K. Rudnick, "Geometric Formulas for Dilution of Precision Calculations," *Navigation*, vol. 37, no. 4, pp. 379–391, 1990.

[17] R. Santerre and A. G. ans Simon Banville, "Geomtery of GPS Dilution of precision: revisited," *GPS Solution*, vol. 21, pp. 1747–1763, 2017.

[18] L. Wanninger, V. Frevert, and S. Wildt, "Der Einfluss der Signalbeugung auf die präzise Positionierung mit GPS," *Zeitschrift für Vermessungswesen*, vol. 125, no. 8, pp. 8–16, 2000.

[19] R. Dach, S. Schaer, D. Arnold, L. Prange, D. Sidorov, P. Stebler, A. Villiger, and A. Jäggi, "CODE final product series for the IGS," *Published by Astronomical Institute, University of Bern*, 2018.

[20] W. Gurtner and L. Estey, "RINEX - The Receiver Independent Exchange Format," *International GNSS Service (IGS), RINEX Working Group and Radio Technical Commission for Maritime Services Special Committee 104 (RTCM-SC104)*, 2015.

[21] S. Hilla and M. Cline, "Evaluating pseudorange multipath effects at stations in the National CORS Network," *GPS Solutions*, vol. 7, no. 4, pp. 253–267, mar 2004. [Online]. Available: https://doi.org/10.1007%2Fs10291-003-0073-3

[22] A. Bilich and K. M. Larson, "Mapping the GPS multipath environment using the signal-to-noise ratio (SNR)," *Radio Science*, vol. 42, no. 6, nov 2007. [Online]. Available: https://doi.org/10.1029%2F2007rs003652